Science Reports, Institute of Geoscience, University of Tsukuba,
Section A (Geographical Sciences), Vol. 21, 2000, pp. 1-21.

A Study of Deterministic Predictability for the Barotropic Component of the Atmosphere

H. L. TANAKA and Daisuke NOHARA*

Abstract

In this study, deterministic predictability for the vertical mean state (i.e., barotropic component) of the atmosphere is examined by conducting perfect-twin model experiments. First, we evaluated the barotropic-baroclinic interaction with observed data. Given the interactions as the external forcing, a barotropic model is integrated with respect to time. It is demonstrated that such a pseudo-perfect model accurately follows the trajectory of the real atmosphere for a hundred days.

Next, perfect-twin model experiments are conducted for the barotropic model superimposing small random error on the initial state. It is found that the predictability increases by 10 days when the initial error energy is reduced to 1/10. Since the model predicts the vertical mean quantities, the initial error may be reduced in proportion to the square root of the total number of the sample data. The result suggests that the vertical mean state may be predictable beyond two weeks "if" we can have a perfect model with sufficient number of observations in the vertical.

The perfect-twin model experiments are also conducted with internal model physics to confirm the long predictability for the barotropic component of the atmosphere. Sample forecasting experiments are carried out for the real atmosphere. The result suggests that the predicting vertical mean of the atmosphere can be one of the viable approaches to the medium-range weather prediction, provided that the barotropic-baroclinic interactions are accurately parameterized.

1. Introduction

A medium-range numerical weather prediction has been hampered by the prediction barrier caused by the chaotic nature of nonlinear fluid systems. According to the pioneer work by Lorenz (1963; 1969), formally deterministic fluid systems having multiple scales of motion are observationally indistinguishable from indeterministic systems, due to the existence of chaos. The basic principle of chaos is a rapid growth of small initial errors, which deviates from the true trajectory of the solution. Lorenz showed that each scale of motion possesses an intrinsic finite range of predictability; cumulus-scale motions can be predicted by about one hour, synoptic-scale motions by a few days, and global-scale motions by a maximum of two weeks. It is our contention that deterministic medium-range forecasting is impossible beyond two weeks of the chaotic barrier, even if we can have a perfect prediction model. At present, the useful deterministic predictability with operational numerical weather prediction models is 7 to 10 days (Lorenz 1985; Dalcher

* Doctoral Program in Geoscience, Universty of Tsukuba

and Kalnay 1987; Kalnay et al. 1990; Kalnay et al. 1998).

The predictability might be extended by predicting averaged quantities. Anomaly correlation is better for planetary waves than for synoptic or short waves, when those waves are separated (e.g.,Vallis 1983; Shukla 1985; Bengtsson 1985). This implies that spatial averaging increases predictability. Miyakoda et al. (1986), on the other hand, constructed a one-month prediction model which predicts 5-day or 10-day mean field by separating slowly moving low-frequency variability from unpredictable high-frequency eddies. Here, the contribution from transient eddies interacting with the low-frequency part appears to be the key issue.

An attempt was also made to construct a 2-D model that predicts the zonal mean state in the meridional height section (e.g., Satoh 1994). The model needs to parameterize zonal eddies which accelerate zonal mean flows. The role of baroclinic wave activities induced by baroclinic instability was extensively investigated in the context of baroclinic adjustment (Stone 1978). Transformed Eulerian Mean Equations were derived, and Eliassen-Palm flux divergence was extensively analyzed as a unique eddy contribution term which interacts with zonal motions (Edmon et al. 1980). However, the parameterization of such an eddy contribution is far from satisfaction. Recently, the main approach to medium-range weather forecasting is the ensemble prediction, in which a number of ordinary numerical model predictions are averaged to reduce the uncertainty caused by chaos (e.g., Toth and Kalnay 1997; Molteni et al. 1996). Although this method extended predictability to some extent, the chaotic nature of nonlinear fluid systems still limits its effectiveness.

One viable approach which has not pursued much to extending predictability by averaging is to predict the vertical mean of the state variables. In this method, primitive equations are averaged with respect to the vertical, and the resulting barotropic component of the atmosphere is predicted. The barotropic-baroclinic interaction appears to be the key issue to be parameterized. In general, the low-frequency variabilities, such as blocking phenomenon, PNA-like teleconnections, and Arctic Oscillation (see Thompson and Wallace 1998) are characterized by their barotropic structures. Atmospheric blocking has long been a major concern in medium-range forecasting due to its long life time beyond two weeks. Understanding and predicting atmospheric blocking is expected to improve the forecasting skill.

Recently, we have developed a new type of barotropic general circulation model derived from a 3-D spectral primitive equation with a basis of vertical normal modes and Hough harmonics (see Tanaka 1991; Tanaka 1998). The model predicts the vertical mean state (barotropic component) of the state variables. The barotropic component in this model is defined by the following vertical transform weighted by the vertical normal mode function G_0:

$$(u,v,\phi)_0^T = \frac{1}{p_s}\int_0^{p_s}(u,v,\phi')^T G_0 dp. \qquad (1)$$

Here, $(u,v,\phi')^T$ is a column vector containing the state variables of wind speeds and geopotential deviation from the global mean. Since the vertical structure function for the barotropic mode G_0 is approximately constant with respect to the vertical, the method is equivalent to predict the vertical mean state of the primitive equations. In this model, baroclinic instability is parameterized as a major contribution to the baroclinic-barotropic interactions. It is demonstrated that the model can simulate realistic blocking at the right location and structure with the right behavior. According to the results by Tanaka (1998), the blocking in the model is caused by the inverse energy cascade from synoptic eddies to planetary waves in the wavenumber space, consistent with eddy straining hypothesis in the physical

space (Shutts 1986). Therefore, it is interesting to next investigate the predictability of the model which predicts the vertical mean state of the atmosphere.

Predictability of the quasi-geostrophic (QG) barotropic model was investigated by some researchers. Basdevant et al. (1981) showed that the presence of Rossby wave regime, separated by the Rhines scale (Rhines 1975), increases the predictability due to inhibitation of nonlinear error growth at the anisotropic part of the Rossby wave regime. Vallis (1983) showed that the predictability becomes 25 days with his QG barotropic model. He suggests that baroclinic instability induced by the two-layer QG model substantially reduces the predictability. Holloway (1983) suggests that inclusion of finite equivalent depth, as well as the β effect, increases the predictability of the QG barotropic model four time longer than previous estimates based on 2-D turbulence by Leith (1971) and Leith and Kraichnan (1972). The barotropic model in this study is based on vertically truncated primitive equations and is clearly different from the former (QG) barotropic models. If we can extend the limit of the deterministic predictability by the vertical averaging with a suitable additional forcing, the method would be useful for the medium-range weather forecasting.

The purpose of this study is to examine the predictability of the barotropic component of the atmosphere using the barotropic model by Tanaka (1998) by conducting perfect-twin model experiments. The model sensitivity to the initial error is examined for certain blocking events in the real and model atmospheres. First, we evaluate the barotropic-baroclinic interactions based on the observed data during the event of a pronounced blocking in the north Pacific. Given the barotropic-baroclinic interactions as the external forcing, the perfect-twin model experiments are conducted for the blocking life-cycle in the real atmosphere. Next, we integrate the barotropic model with the parameterized baroclinic instability to generate large-scale persistent blocking in the model atmosphere. When a realistic blocking appears, we superimpose a small error on the solution trajectory two weeks before the blocking formation. We can see whether the robust blocking life-cycle in the model atmosphere is predictable or not from two weeks in advance using the perfect-twin model with noise in the initial data. Finally, some examples of actual predictions of the real atmosphere are presented using the barotropic model with a suitable external forcing.

Note that any random observation error contained in the state variables can be reduced for the vertical mean of Eq. (1) in proportion to the square root of the number of sample data. Hence, predicting the vertical mean states can be a viable approach to medium-range weather prediction. The relation between the magnitude of the initial error and the predictability limit is investigated and discussed in the Concluding remarks.

2. Model and data

The model description is detailed in Tanaka (1991) and Tanaka (1998), so a brief description is presented here. A system of primitive equations of the atmosphere with a spherical coordinate may be reduced to three prognostic equations of horizontal motions and thermodynamics for three dependent variables of $U=(u, v, \phi')^T$. Here, u and v are zonal and meridional components of horizontal velocity. The variable ϕ' is a departure of local isobaric geopotential from the global mean reference state, and the superscript T denotes a transpose. Using a matrix notation, these primitive equations may be written as

$$M\frac{\partial U}{\partial t}+LU=N+F. \qquad (2)$$

Here, t is time, and the left-hand side of (2) represents linear terms with matrix operators M and L and the dependent variable vector U. The

right-hand side represents a nonlinear term vector N and a diabatic term vector $F=(F_\lambda, F_\varphi, F_Z)$ which includes zonal and meridional components of frictional force and a diabatic heating rate.

In order to obtain a system of spectral primitive equations, we expand the vectors U and F in 3-D orthonormal basis functions. After a proper diagonalization of the linear terms on the left hand side, we may obtain a system of 3-D spectral primitive equations in terms of a standard form:

$$\frac{dw_i}{d\tau}+i\sigma_i w_i = -i\sum_{jk} r_{ijk}w_j w_k + f_i, \quad i=1,2,3,... \tag{3}$$

where w_i and f_i are the 3-D Fourier expansion coefficients of U and F, τ the dimensionless time, σ_i the eigenfrequency of the Laplace's tidal equation, and r_{ijk} the nonlinear interaction coefficients. The standard expansion basis functions that diagonalize the linear matrices are vertical structure functions (vertical normal modes) and Hough harmonics (horizontal normal modes). The triple indices of zonal wavenumber n, meridional index l, and vertical index m are shortened to a single index i for convenience. There should be no confusion in the use of i for a subscript, even though it is used also for the imaginary unit.

The spectral primitive equation (3) was integrated in time by Tanaka (1995) for a study of a life-cycle of nonlinear baroclinic waves. The result clearly showed that synoptic waves draw energy from baroclinic components of the atmosphere and feed energy to the barotropic components. It was found that the important baroclinic-barotropic interactions are accomplished by baroclinic instability (e.g., Salmon 1980; Hoyer and Sadourny 1982; Tanaka and Kung 1988).

In the 3-D spectral representation, the vertical expansion basis functions may be divided into barotropic and baroclinic components. We may construct a simple spectral barotropic model, using only the barotropic components (m=0) of the Rossby modes, by truncating all the baroclinic modes and high-frequency gravity modes (see Kasahara 1977).

$$\frac{dw_i}{d\tau}+i\sigma_i w_i = -i\sum_{jk} r_{ijk}w_j w_k + f_i,$$
$$i=1,2,3,...(\mathrm{m}=0), \tag{4}$$

where the indices of the subscripts run only for the barotropic modes. The zonal and meridional wave truncation of the present model is equivalent to rhomboidal 20 with an equatorial wall. The degree of freedom of the system is reduced enormously by these truncations. The spectral equation for such a barotropic model (4) has the same form as for the baroclinic model equation (3), except for the fact that the barotropic-baroclinic interactions should be included formally in the external forcing f_i.

In the first part of this study, the external forcing f_i is evaluated as the residual of (4) using the observed state variables w_i. The dataset used in this study is the operational global analysis provided by the Japan Meteorological Agency for January to March, 1997, which is referred to as GANAL/JMA data. The dataset contains four-times daily (0000, 0600, 1200, and 1800Z) meteorological variables of horizontal wind vector (u,v) and geopotential ϕ at 1.25° longitude by 1.25° latitude grids on 17 mandatory vertical levels of 1000, 925, 850, 700, 600, 500, 400, 300, 250, 200, 150, 100, 70, 50, 30, 20, and 10 hPa.

Given the external forcing interpolated on one-hour intervals, the model equation (4) is then integrated with respect to time, starting from initial states of w_i on certain days during the analysis period. Since the perfect value of f_i is provided when τ and w_i are specified, the model is called a pseudo-perfect model ("P-Model" in short) for the real atmosphere. It is, of course, not the true perfect model, but an imitation of it, since f_i is given from outside, rather than computed internally. We then

superimpose an initial error for the P-Model run to conduct a pseudo-perfect-twin model experiment for the real atmosphere.

From the experiments with the P-Model, we know both of f_i and w_i from the observation. Establishing the functional relation of $f_i(w_i, \tau)$ given w_i and τ is the next subject to close the system. In the second part of this study, the external forcing is estimated within the model considering the following physical processes:

$$f_i=(BC)_i+(TF)_i+(DF)_i+(DZ)_i+(DE)_i, \tag{5}$$

where $(BC)_i$ represents the baroclinic instability, $(TF)_i$ the topographic forcing, $(DF)_i$ the biharmonic diffusion, $(DZ)_i$ the zonal surface stress, and $(DE)_i$ the friction by Ekman pumping. Refer to Tanaka (1998) for the detail of these physical processes. For simplicity, this model is called "B-Model" which has been developed specifically to simulate a realistic blocking. When a pronounced blocking appears in the control run by the B-Model, we conduct a perfect-twin model experiment for the blocking in the model atmosphere. In the experiment run, an initial noise is superimposed on the trajectory of the control run to investigate the growth of the initial noise.

The parameterization of (5) is fundamentally a linear approximation to the true forcing and is never perfect for the real atmosphere even if we know the perfect f_i from the observation. In the last part of this study, we attempt to obtain the best linear fit of the forcing f_i based on 17 years of the global reanalysis data provided by the National Center for Environmental Prediction and National Center for Atmospheric Research (NCEP-NCAR):

$$f_i=\tilde{f}_i+\mathbf{A}_{ij}w_j+\varepsilon_i, \tag{6}$$

where $\tilde{f}_i$ is the climate of f_i with a seasonal change, the unknown linear matrix $\mathbf{A}_{ij}$ may be obtained by the standard method of the least square fitting to minimize the residual of ε_i:

$$\mathbf{A}_{ij}=\overline{f_i' w_j^+}. \tag{7}$$

Here, $f_i'=f_i-\tilde{f}_i$ is the anomaly of f_i, $(\overline{\ })$ is the time mean, and w_j^+ is referred to as pseudo-inverse of w_j defined by

$$w_j^+=w_k^H\,(\overline{w_k w_j^H})^{-1}, \tag{8}$$

where the superscript H denotes a complex conjugate transpause. The model with such a forcing is named as "S-Model" since the forcing is obtained statistically from observation. The application of the S-Model to the real forecasting is demonstrated later in this study. The linear matrix of (7) is computed from the NCEP-NCAR reanalysis for 1979 to 1995, and the real forecasting is carried out for the GANAL/JMA data in 1997 to avoid statistically dependent forecasting.

The S-Model is further improved by adding a complex conjugate term of w_i as:

$$f_i=\tilde{f}_i+\mathbf{A}_{ij}w_j+\mathbf{B}_{ij}w_j^*+\delta_i, \tag{9}$$

where the matrix $\mathbf{B}_{ij}$ may be obtained by minimizing the reminder δ_i by regressing the former residual ε_i:

$$\mathbf{B}_{ij}=\overline{\varepsilon_i\, w_j^{*+}}, \tag{10}$$

using the pseudo-inverse of w_j^*. Here, the terms with $\mathbf{A}_{ij}$ and $\mathbf{B}_{ij}$ represent a down scale and up sclae energy interaction terms.

In the spectral domain, total energy E (sum of kinetic energy K and available potential energy P) is simply the sum of the energy elements E_i defined by:

$$E_i=\frac{1}{2}p_s h_m|w_i|^2, \tag{11}$$

where the dimensional factors p_s and h_m are the surface pressure of the reference state and the

equivalent depth of the atmosphere, respectively. Here, m is 0 since the model contains only the barotropic component of the atmosphere. The difference between the experiment run and the control run, which is referred to as error, is measured quantitatively by the error energy defined as

$$\Delta_i = \frac{1}{2} p_s h_m |w_i - \hat{w}_i|^2, \qquad (12)$$

where w_i is the state variable of the experiment run and $\hat{w}_i$ is that of the control run. The total error energy is the sum of Δ_i over all indices.

The present barotropic model is different from a standard shallow water system in that all possible high-frequency gravity modes have been truncated out. Those gravity modes, if contained in the model, can be a great source of error energy, even though the amplitude itself may be kept small using an advanced technique. The baroclinic component of the atmosphere is also the major source of the error energy associated with the rapid growth of the local baroclinic instability. The present model is unique in that the baroclinic instability is parameterized as an important component of the baroclinic-barotropic interactions. Therefore, strong dynamical instabilities associated both with baroclinic instability and gravity waves have been ruled out from the dynamical core of the mode by truncations of gravity mode basis and baroclinic mode basis. It is therefore intriguing to find whether the vertical mean state of the atmosphere indicates longer predictability than a 3-D local quantity or not.

3. Pseudo-perfect-twin model experiments

Barotropic components of the state variables $(u, v, \phi)_0^T$ are evaluated according to (1) for January 1 to March 31, 1997 using the GANAL/JMA datasets. Figure 1 illustrates the resulting geopotential-height distributions in the Northern Hemisphere at 1200Z on March 7, March 11, and March 14 in 1997. The distribution is similar to 500 hPa height. It is found that the overall features of the westerly jet, planetary waves, and synoptic waves in the general circulation are contained in the barotropic component. The wind field (not shown) is very close to the geostrophic balance, because only the Rossby modes are retained in the state variables w_i in (4) after the spectral truncation. On March 7, a high-index circulation pattern dominates over the Pacific sector with a strong zonal jet. On March 11, a synoptic scale wave appears to develop over the

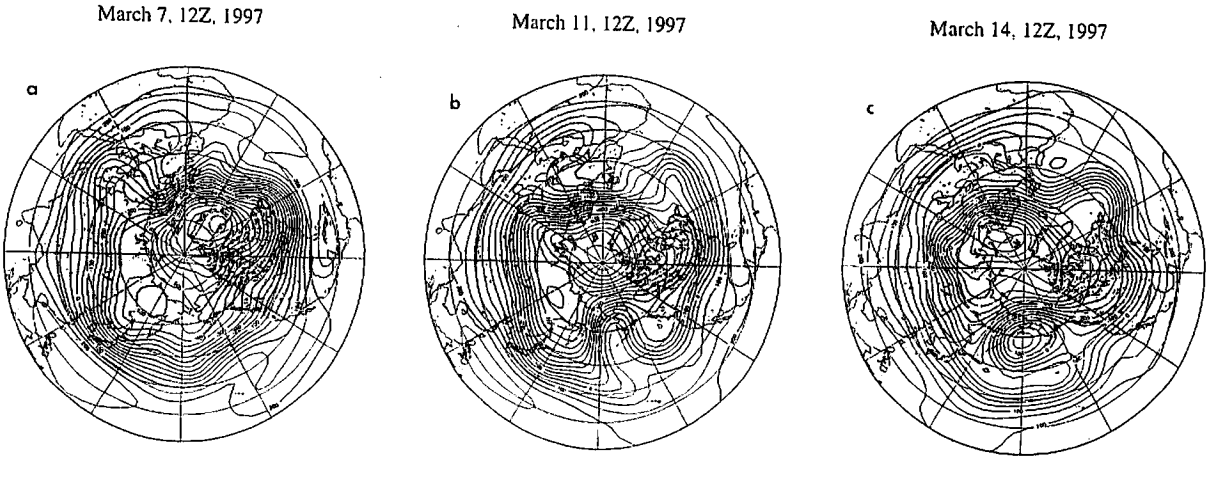

Fig. 1 Distributions of the barotropic component of geopotential height in the Northern Hemisphere at 1200Z on (a) March 7, (b) March 11, and (c) March 14 in 1997 evaluated from GANAL/JMA data. Contour interval is 50 gpm. Large-scale blocking is developing in the north Pacific.

Pacific sector, creating a strong meridional flow. On March 14, a pronounced blocking high establishes over the north Pacific. According to the analysis of the water vapor channel in the GMS-5 satellite, we can see a huge downburst of dry air spreading around the blocking high during this period. Compared with the 500 hPa height, we find that the characteristic features of the blocking high and polar vortex are almost completely retrieved by the barotropic component of the atmosphere. However, the cut-off lows, especially in the south of the blocking high, are projected relatively weak, since those contain a large fraction of baroclinic components. Since the barotropic component contains overall features of the low-frequency variability, predicting this component alone may be still meaningful for medium-range weather forecasting.

Figure 2 illustrates distributions of the mean linear term, nonlinear term and external forcing in the spectral primitive equation (4) for January 1 to March 31, 1997 evaluated from GANAL/JMA dataset. The figures illustrate distributions associated with the geopotential field computed by the inverse Fourier transforms. The forcing F_Z is the inverse Fourier transforms of f_i in (2) and is referred to as barotropic forcing. The contour interval for F_Z is a half of the linear and nonlinear terms. The linear term represents positive tendency of geopotential height over the Pacific Ocean and Atlantic Ocean and negative tendency over north America, Europe, and the Far East, so that the planetary wave propagates westward as a Rossby wave. The mean linear term is approximately balanced with the nonlinear term, and the small residual results in the barotropic forcing F_Z. The mean distribution of F_Z indicates positive values at the west coast of the American and Eurasia continents and negative values at the east coast of those continents. The pattern may be consistent with the vertical motions induced by topographic uplift (e.g., Ringler and Cook 1999).

The longitude-time section of the barotropic forcing F_Z along 58°N is illustrated in Fig. 3 for March 7 to 20, 1997. The diurnal variation has been filtered out in the figure. The distribution of forcing is, in general, noisy and complicated in space and time. Associated with the development of the Pacific blocking in Fig. 1, large positive forcing of F_Z is seen over 170°E for days 8 through 14. The positive forcing shows retrogression to the west after the mature stage of the blocking. The similar Hovmöller

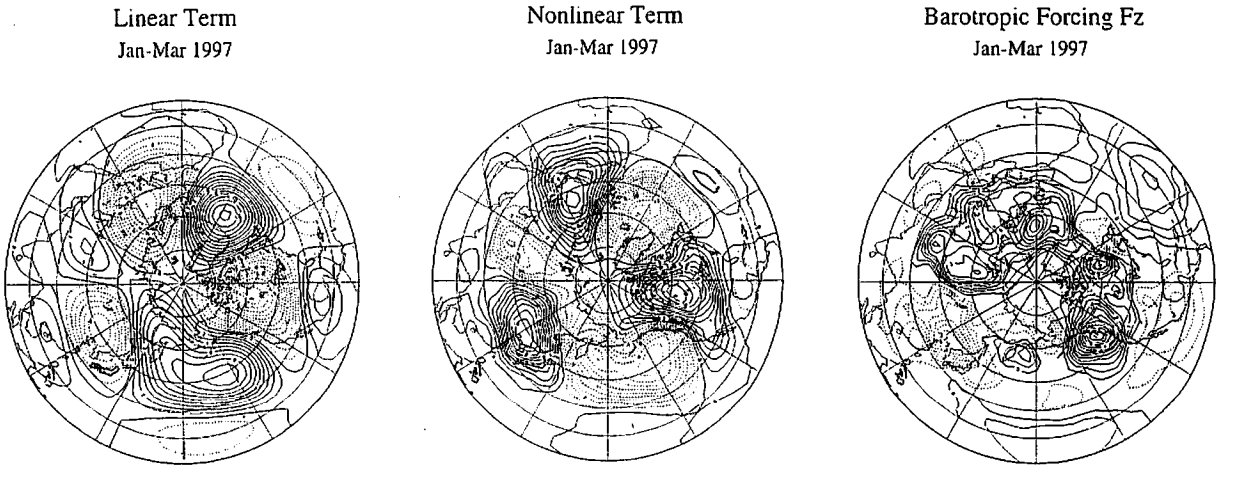

Fig. 2 Distributions of the mean linear term, nonlinear term and barotropic forcing F_Z in the geopotential field of the spectral primitive equation (4) during January 1 to March 31, 1997 evaluated from GANAL/JMA data. The contour interval is 1.0 ($\times 10^{-3}$ m^{2}s^{-3}) for linear and nonlinear terms and is 0.5 for F_Z.

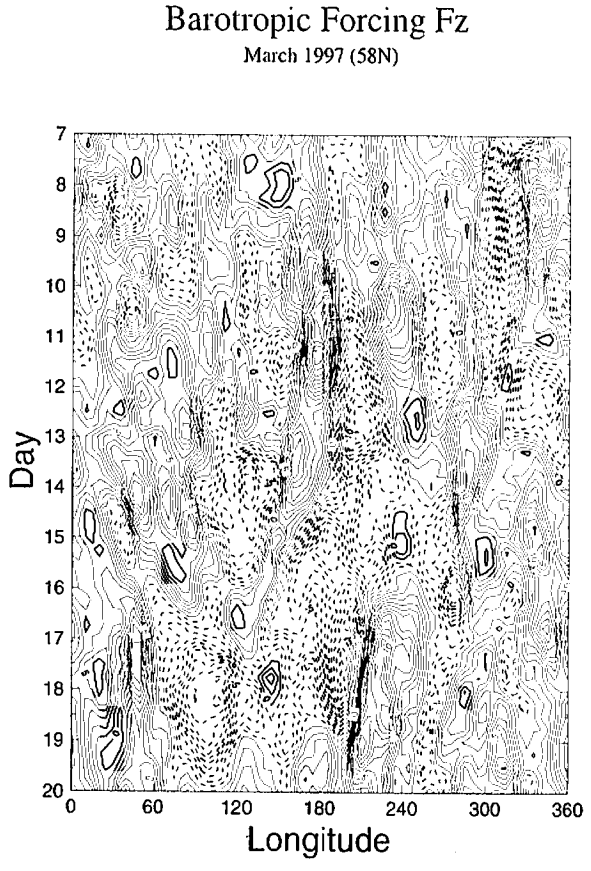

Fig. 3 Longitude-time section of barotropic forcing F_Z along 58° N for March 7 to 20, 1997 evaluated from GANAL/JMA data. The contour interval is 1.0 ($\times 10^{-3}$ $m^2 s^{-3}$).

diagrams for the linear and nonlinear terms (not shown) indicate clear progression of synoptic-scale eddies advected by the westerly. It is interesting to note that such progression is not seen for the barotropic forcing.

Establishing the functional relation of $f_i(w_i, \tau)$ given w_i and τ is our ultimate goal for constructing the perfect model of the real atmosphere. Since it is extremely difficult, $f_i(w_i, \tau)$ is provided from observations in the P-Model. Therefore, this model is not a true perfect model, but a pseudo-perfect-model run for the real atmosphere, because the perfect external forcing f_i is provided at every time step. Given the time series of the external forcing evaluated from observations, the model equation (4) is integrated from the initial data at 1200Z, March 7, 1997.

According to the result of the P-Model run in Fig. 4, the life-cycle of the pronounced blocking described in Fig. 1 is perfectly reproduced by this model. In fact, we demonstrated that the time behavior of the real atmosphere can be reproduced, even for the entire three months of the analysis period, starting from the initial value on January 1, 1997. Further analysis shows that the model atmosphere behaves almost exactly as the real atmosphere up to a hundred days when the perfect external forcing

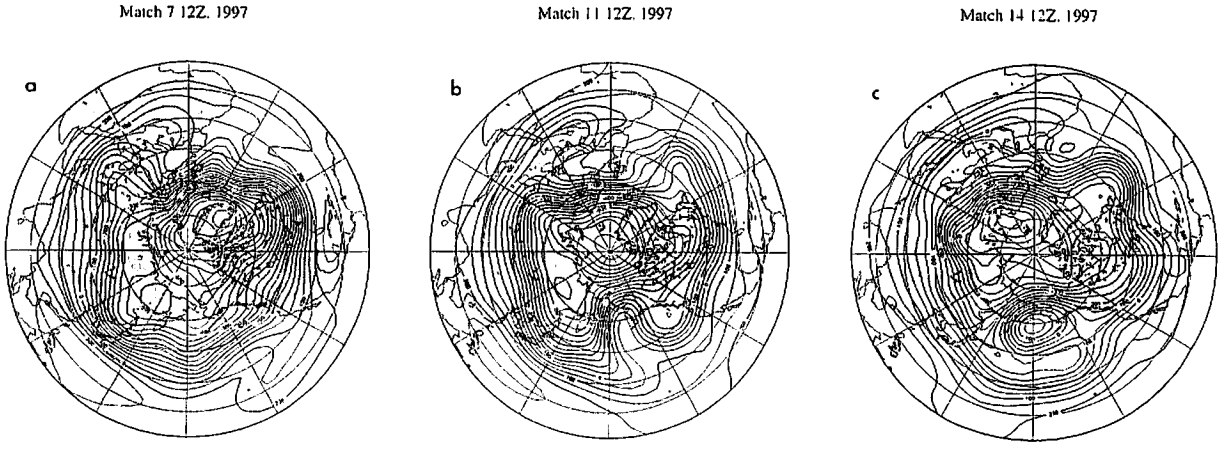

Fig. 4 Distributions of the geopotential height for the P-Model run at 1200Z on (a) March 7, (b) March 11, and (c) March 14 in 1997. The model equation (4) is integrated from 1200Z on March 7 given the diagnostically evaluated external forcing f_i.

is provided. The result may be non-trivial in reference to our current understanding of chaos. Since the model should contain more than an infinitesimal noise in the numerical procedures of the time integration, the noise ought to amplify rapidly to abandon the forecast, according to the theory of chaos. However, what we have found from this experiment is that the initial value problem perfectly follows the real atmosphere for a hundred days, as long as the correct external forcing is provided.

In order to examine the growth of initial error, we integrate the P-Model giving small noise on the initial data. The run is referred to as a pseudo-perfect-twin model experiment. Figure 5 illustrates the mean energy spectrum evaluated from (11) for n=1 to 15, using the ECMWF global analysis (after Tanaka and Kimura 1996). The abscissa denotes a westward phase speed of a Rossby mode $c_i=|\sigma_i|/n$. The larger the horizontal scale of a Rossby mode is, the larger the westward phase speed c_i is. Namely, c_i represents a 3-D scale of a normal mode by means of the wave dispersion relation (see Baer 1972). The energy spectrum for the same zonal wavenumber n is connected by a dotted line since the Hough modes are solved for each n. The largest-scale Rossby mode (so-called 5-day wave of n=1) propagates westward with 5-day period as expected from the normal mode theory. In contrast, the energy levels of the shorter waves (smaller c_i) obey a turbulent-like power slope indicating a dominant nonlinearity. The turbulence regime and the Rossby wave regime are separated by the Rhines scale (Rhines 1975) where energy peaks appear in Fig. 5.

In Fig. 5, the dashed line describes a white noise superimposed on the initial data, plotted in the same frame of the mean energy spectrum of the barotropic atmosphere. The white noise has a random phase around the complex Fourier expansion coefficients of the control run, and the total amount of noise energy is set to 2% of the total barotropic energy of the atmosphere. The ratio increases to 10% when only the zonal eddies (n>0) are compared. Since it is the energy ratio of the noise, it corresponds to much larger ratio of the observational error if we take its square root. Hereafter, we refer to this ratio as 10% error. Evidently, the noise level is higher than the observed energy spectrum for short waves of n < 15, implying that those short waves have more than 100% initial error. The

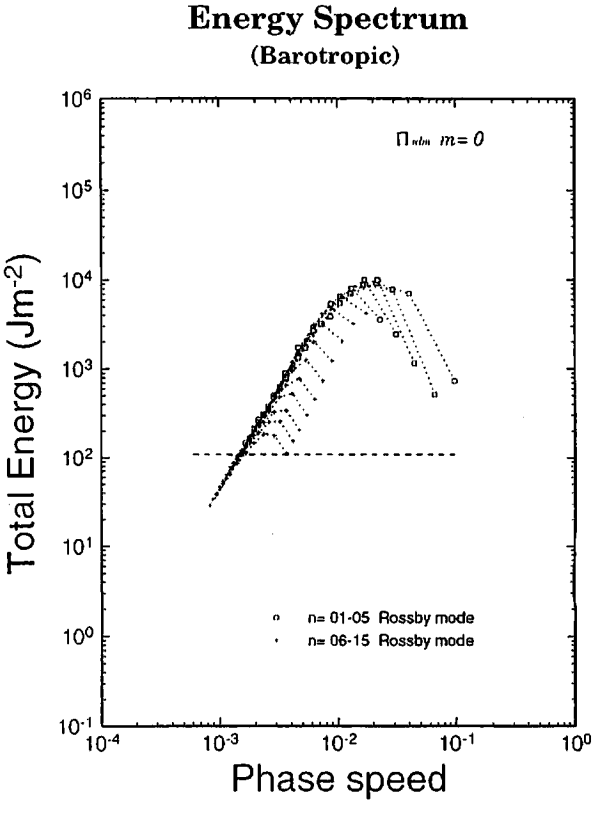

Fig. 5 Mean spectral distributions of total eddy energy (Jm^{-2}) of the barotropic atmosphere evaluated by the ECMWF global analysis (after Tanaka and Kimura, 1996). The abscissa denotes a phase speed of Hough modes $c_i=|\sigma_i|/n$ which may be considered as a 3-D scale index of the mode by the Rossby wave dispersion. Also plotted by dashed line is the initial random white noise used for the perfect-twin model experiment run. The total amount of the error energy is set at 10% of the total eddy energy in the figure.

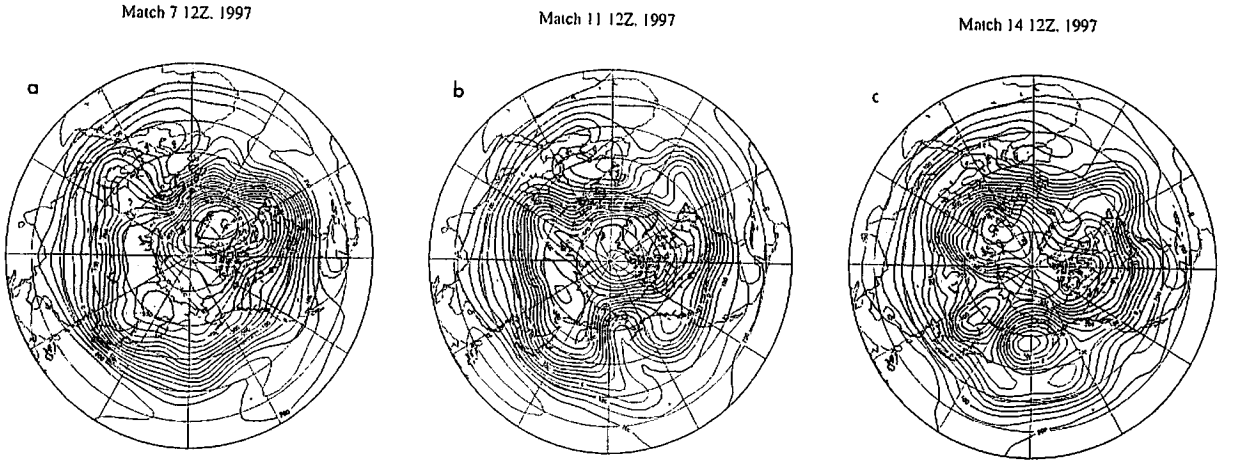

Fig. 6 As in Fig. 4 but for the experiment run with the initial error for the P-Model. In this experiment, a random white noise in Fig. 5 is superimposed on the initial data at 1200Z, March 7, 1997.

noise amounts to about 30 m in geopotential height, which may be greater than the (vertical mean) observational error.

Superimposing the random noise on the initial data, the model equation (4) is integrated again from the initial data at 1200Z, March 7, 1997. Figure 6 illustrates the result of the geopotential height for the pseudo-perfect-twin model experiment. As in Fig. 1, zonal flow is replaced by meridional flow on March 11 and the pronounced blocking appears on March 14. The result demonstrates that the blocking may be predictable one week in advance, even if the initial data contain 100% error for the short waves, as long as the model error is sufficiently small.

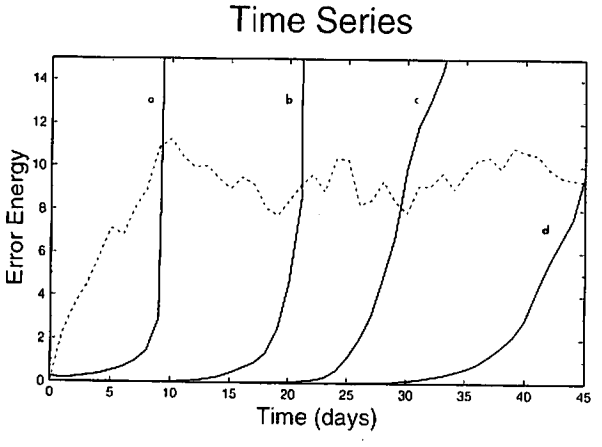

Fig. 7 Growth of error energy for various amount of initial error. The line (a) stands for the 10% white noise as shown in Fig. 5, (b) for 1%, (c) for 0.1%, and (d) for 0.01%, respectively. Also plotted by dashed line represents the error growth of the persistence forecast started from January 1, 1997.

The model sensitivity to the initial noise is further examined in Fig. 7 for various amounts of initial white noise superimposed on January 1, 1997. The lines stand for the growth of error energy in (12) with the units of 10^4 J m^{-2} for the case of (a) 10% white noise as described in Fig. 5, (b) for 1%, (c) for 0.1%, and (d) for 0.01%, respectively. Also plotted by the dashed line is the error growth for the persistence forecast started from January 1, 1997. Since the model predicts the vertical mean rather than a local quantity in the 3-D atmosphere, observational error can be reduced in theory for a large number of the vertical observations. In those experiments, the initial error grows slowly at first, then it diverges suddenly when the error energy reaches 1/10 of the saturation level specified by the persistence forecast. The diverging error energy is reasonable since the external forcing is predetermined, no matter how the state variable evolves. The result is an important clue to the relation between the initial

noise and the predictability. It is found that the predictability increases 10 days when the initial error energy decreases to 1/10. Namely, the predictability limit is inversely proportional to the logarithm of the error energy level. The predictability limit extends up to a hundred days when no error is superimposed in the pseudo-perfect-twin model as mentioned before.

The same experiments as in Fig. 7 are repeated 50 times using NCEP-NCAR reanalysis to increase the statistical confidence. The result supports the hypothesis such that the predictability has no upper bound when the initial error approaches zero as pointed out by Lorenz (1963) for a 2-D turbulent flow.

4. Perfect-twin model experiments using the B-Model

In this section, a long-term integration of the model equation (4) was first carried out for a few years as a control run, using the internally calculated external forcing (5). The forcing may be too simple compared with the complexity of the real atmosphere. Yet, we can improve each of the physical process of the B-Model based on the knowledge of the true forcing f_i evaluated for the P-Model in the previous section.

The initial state of the B-Model is an axisymmetric flow. Disturbances are soon excited by topographic forcing, and the eddy is saturated at an equilibrium energy level about 20 days after the time integration. Some pronounced blockings occasionally appear in the model atmosphere, especially over the north Pacific and north Atlantic sectors. In the following, we examine a typical Pacific blocking that occurred around 955 model day, which was extensively analyzed in Tanaka (1998).

Then, in the experiment run of the perfect-twin model, we superimpose a small error on the initial data and integrate it in parallel with the control run. Figure 8 illustrates the spectral distribution of the mean total energy E_i of the B-Model for n= 1 to 20 during 101-1000 days. Also plotted by dashed line is the initial error-energy level. The spectral features of the model atmosphere agree well with observations in Fig. 5, although the model contains less energy than observation for short waves. Since the mature stage of the blocking is around day 955, the initial data for the experiment run is set on day 941, i.e., two weeks before the mature stage of the blocking.

Figure 9 illustrates the geopotential height of the initial date on day 941 of the control and experiment runs, and the difference between the two. We note that no blocking is detectable over the north Pacific on day 941, but amplified zonal wavenumber 6 is superimposed on the mid latitude westerlies. The random error superposed on the control run shows at most 30 m in the magnitude of the geopotential height,

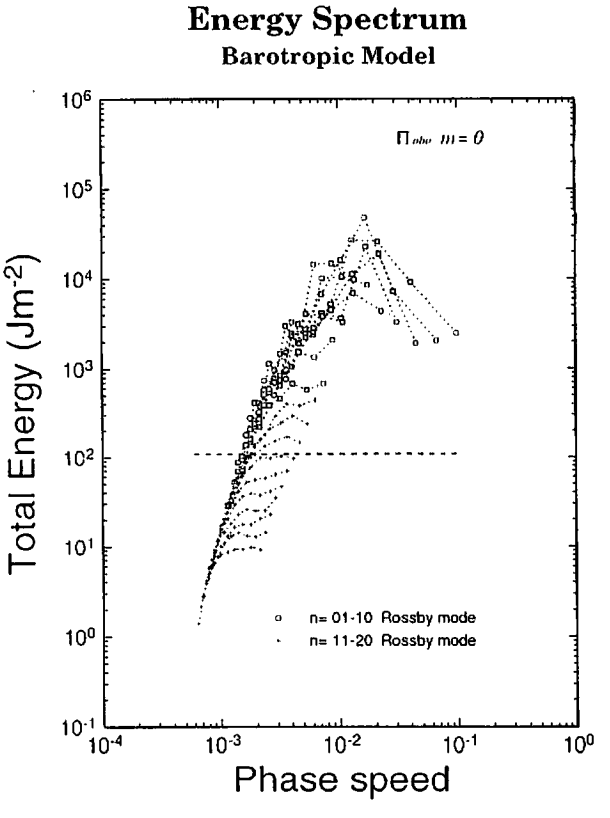

Fig. 8 As in Fig. 5, but for the B-Model during days 101 to 1000. Energy spectrum is plotted for zonal wavenumbers n=1 to 20.

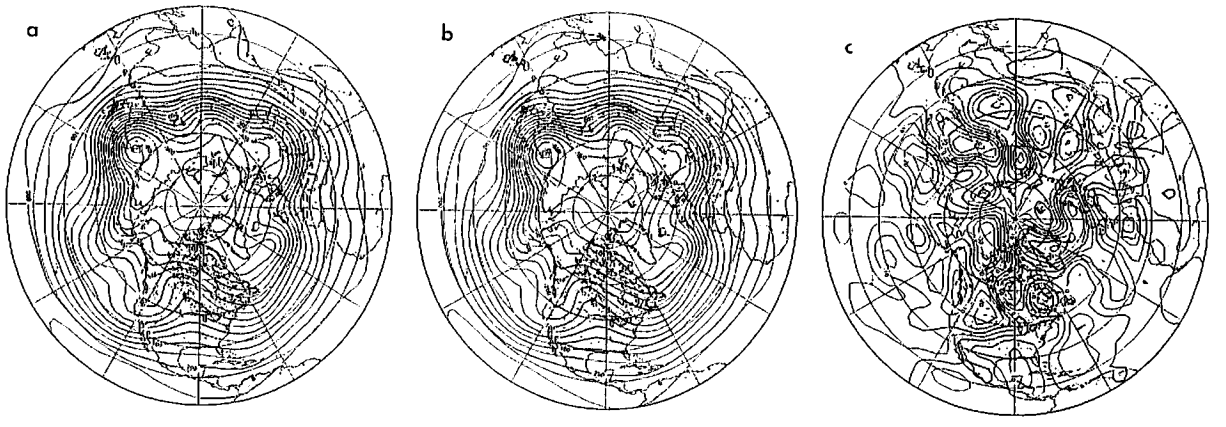

Fig. 9 Distributions of geopotential height for the perfect-twin model experiment with the B-Model on day 941 for (a) the control run, (b) the experiment run with initial noise, and (c) the difference between the two runs (b-a). The contour intervals are 50 m for height and 5 m for the difference.

which is considerably large.

Figure 10 compares the geopotential height for two runs on day 955; 14 days after the beginning of the experiment run. We confirm that the pronounced dipole blocking over Alaska is successfully simulated by the experiment run, despite the initial error superimposed. The location, configuration, and strength are all satisfactory for the dipole blocking, as well as those of troughs and ridges in the rest of the domain. The prediction error is still of the order of 50 m. It should be mentioned that no notable error growth occurs during the two weeks of the experiment run.

The perfect model experiment with the B-Model is further extended to day 962, three weeks after the beginning of the experiment. The result is presented in Fig. 11. The experiment run adequately simulates the whole sequence of the life-cycle of the Pacific blocking, as evidenced from the agreement of the two geopotential fields on day 962. When the blocking is fading out to an ordinary ridge over the West Coast of the United States, the error attains to 100 m in high latitudes and continues to increase, even three weeks after the beginning of the experiment. The deterministic prediction for three weeks is still meaningful within the model atmosphere for this specific blocking event.

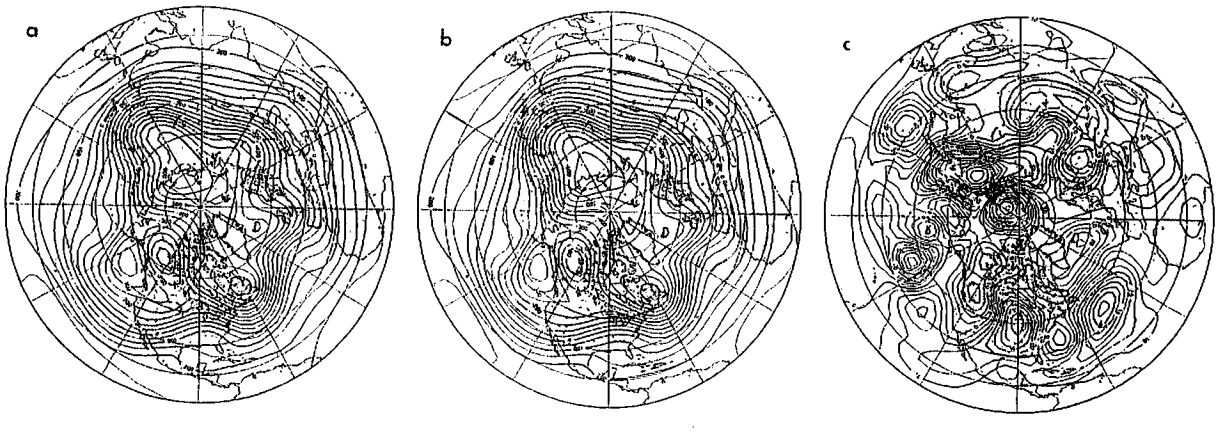

Fig. 10 As in Fig. 9, but for the day 955, i.e., 14 days into the forecast. Note that the pronounced dipole blocking over Alaska is successfully simulated by the experiment run.

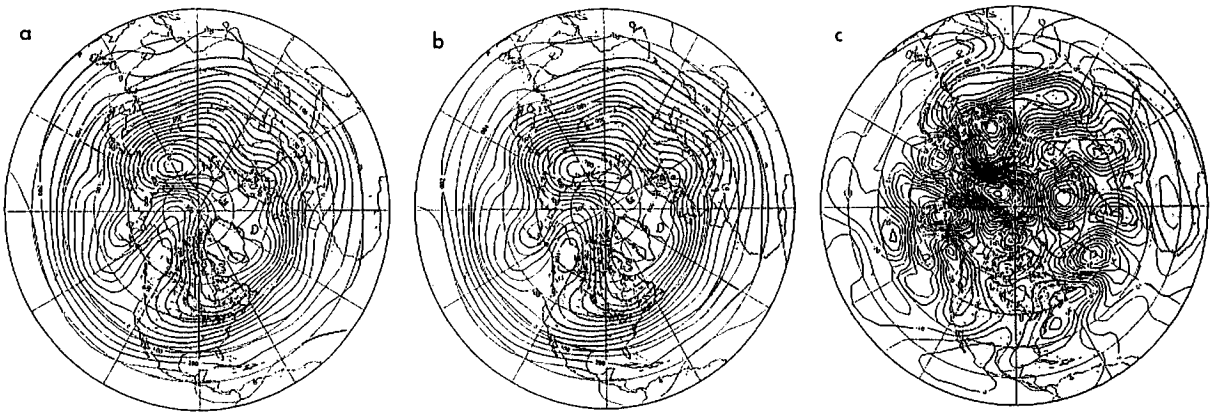

Fig. 11 As in Fig. 9, but for the day 962, i.e., 21 days into the forecast.

The sequence of the development, maintenance, and decay of the blocking event is expressed in Fig. 12a, using a Hovmöller diagram of barotropic potential vorticity q along 58° N for days 945 to 980. The blocking high is characterized by a low value of q (white area) and the troughs by a high value of q (black area). As described by Tanaka (1998) the progressive free waves excited by the baroclinic instability approach the stationary ridge induced by the topography near 180° E and break there. The ridge of the quasi-stationary planetary wave interacts with a progressive free wave and captures it at a fixed geographical location to initiate a blocking. Subsequent free waves are then blocked by the blocking and stretched in a

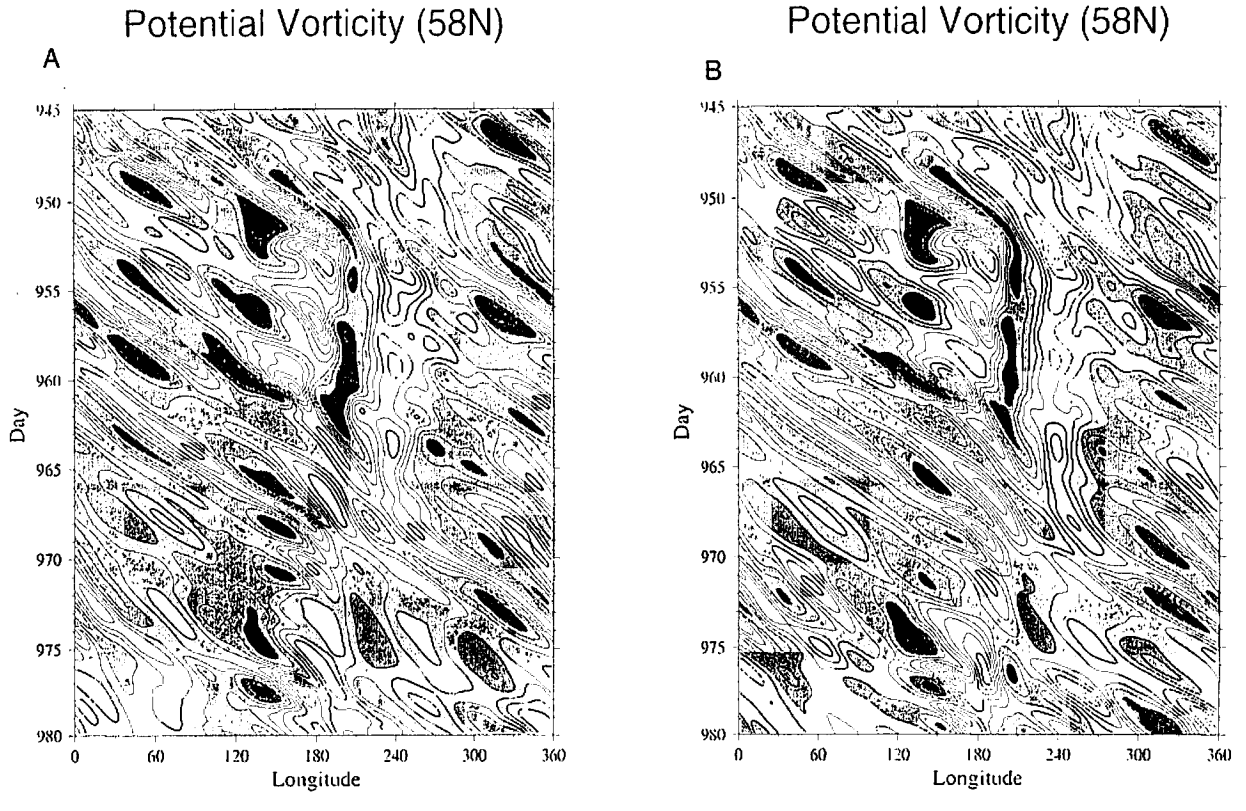

Fig. 12 Longitude-time section of potential vorticity q (PV units) along 58° N during days 945 to 970 for (a) the control run and (b) the experiment run with the B-Model.

north-south direction. An eddy straining mechanism supplies fresh low q into the blocking high during 950 to 965 days. When the lifetime of the block is over, the pair of high and low q is swept away downstream.

We can clearly understand the formation of blocking by a breaking Rossby wave and the maintenance by the eddy straining mechanism as discussed in Tanaka (1998). Figure 12b illustrates the same Hovmöller diagram of q, but for the experiment run with an initial error starting from day 941. Evidently, the entire sequence of development, maintenance, and decay of the blocking event is simulated rather accurately, despite the considerable amount of the initial error.

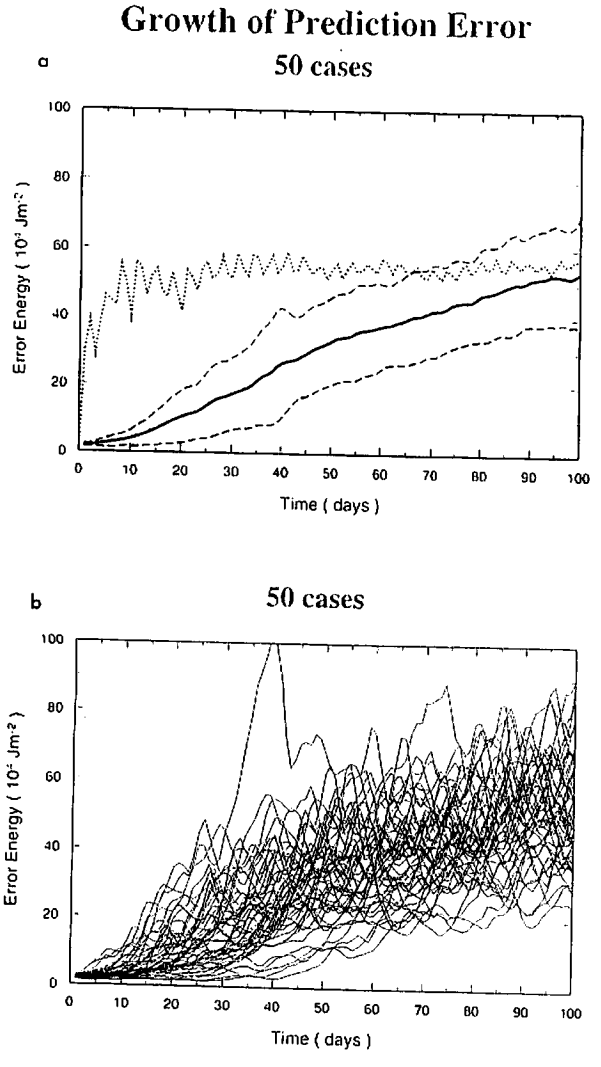

Fig. 13 (a): Mean growth of the error energy for the 50 samples of the perfect-twin model experiments with the B-Model (solid line), its standard deviation (dashed lines), and the mean error energy of a persistence forecasting (dotted line) over the 100 days into the forecasts. (b): The 50 individual samples of growing error energy for the perfect-twin model experiments with the B-Model. Units are $10^4 \mathrm{Jm}^{-2}$.

The perfect-model experiment using the B-Model is repeated for 50 cases to increase the statistical confidence of this model's predictability. Initial random error (see Fig. 8) is superposed on a certain day of the control run, and the experiment run is integrated with initial error for 100 days. Such a 100-day prediction test is repeated 50 times under the similar experimental setting. Figure 13a illustrates the mean growth of the error energy for the 50 randomly sampled forecasts. The range of one standard deviation is plotted by dashed lines. Also plotted by dotted line is the mean error growth by persistence forecasting evaluated for the analysis period. Compared with the saturation level by the persistence forecasting, the forecast error of the model grows very slowly and attains the saturation level about 100 days after the initial date. Figure 13b plots the result of all 50 individual experiments. Although there are cases that attain the saturation level before 100 days, some experiments indicate extremely slow growth of the error energy. Evidently, the slow error growth demonstrated for a blocking event in the previous section is not an accident for a specific case, but a real feature of the present model.

Since the predictability limit is often measured by an anomaly correlation instead of the MSE (error energy in this study), we computed the anomaly correlation of the geopotential height between the control run and the experiment run. Figure 14a illustrates the mean anomaly correlation of geopotential heights for the 50 randomly sampled forecasts.

The range of one standard deviation is plotted by dashed lines. When the anomaly correlation drops to 0.6 and below, the forecasting is considered as meaningless. Therefore, the intersect of the dropping anomaly correlation and the 0.6 line is defined as the predictability limit. The result shows that the predictability limit of the B-Model is 35 days. Figure 14b plots the results of all 50 individual experiments. The shortest predictability is about 15 days, whereas the longest predictability is about 70 days.

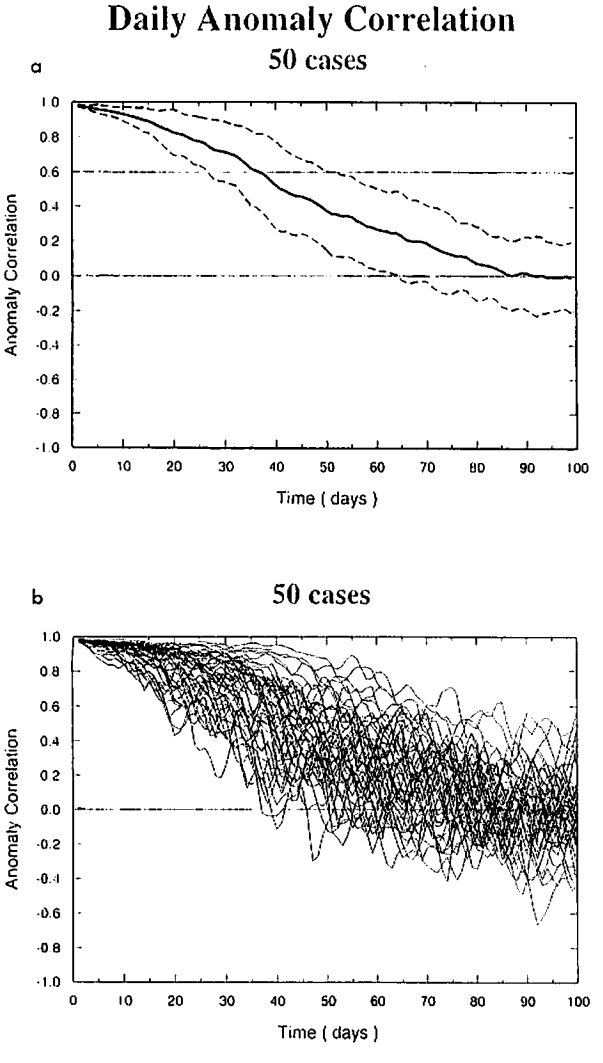

Fig. 14 (a): Mean anomaly correlation of geopotential heights for the 50 samples of the perfect-twin model experiments with the B-Model (solid line) and its standard deviation (dashed lines) over the 100 days into the forecasts. (b): The 50 individual samples of the anomaly correlation for the perfect-twin model experiments with the B-Model.

The same experiments are repeated using red noise initial error instead of white noise. Here, the red noise contains larger error in planetary waves in proportion to the observed energy level, while the total amount of noise energy is set to 10% as in the case of the white noise. We confirmed that the results of the very-long predictability of the model are unchanged for the red noise case (not shown). The relation between the predictability limit and the initial error energy levels is also investigated for the B-Model. It is shown that the predictability increases 25 days when the initial error energy decreases to 1/10. The logarithmic relation discussed for the P-Model in Fig. 7 certainly holds also for the B-Model indicating longer predictability.

5. Forecast experiments using the S-Model

It is noted that the parameterization of the baroclinic instability by the B-Model generates right amount of synoptic eddies, which is essential in the model atmosphere to excite the realistic blocking by means of the inverse energy cascade. It appears, however, that the parameterization is not satisfactory with regards to the forecasting of the real atmosphere. Baroclinic instability occurs locally in response to the local baroclinicity. The spectral approach to excite local disturbance results in considerable error. A slight difference in phase speed of the growing eddies also causes another source of error.

Since the parameterization of (5) is basically a combination of linear matrices, one approach to the real forecasting is to find out the best fit of a single matrix $\mathbf{A}_{ij}$ in (6) from observation. Figure 15 illustrates the seasonal variation of the normal value of $\tilde{f}_i$ in (6) of the S-Model, evaluated by the 17 years of the NCEP-NCAR

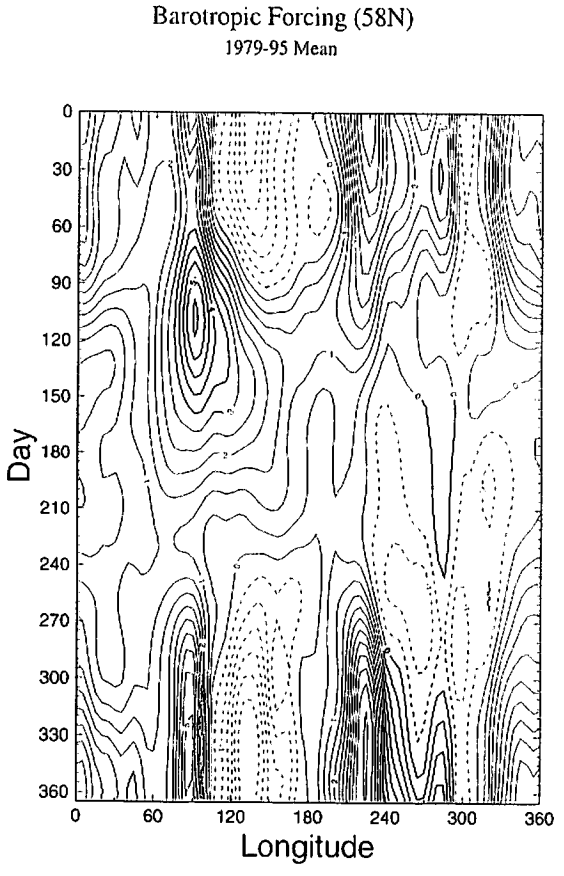

Fig. 15 Seasonal variation of the normal external forcing $\tilde{f}_i$ in (6) for the S-Model evaluated from 17 years of NCEP-NCAR reanalysis. The contour is for the barotropic forcing F_Z with the interval 0.5 ($\times 10^{-3}$ m^{2}s^{-3}).

reanalysis. The values are for the barotropic forcing F_Z as in Fig. 3. The first four harmonics with respect to time are synthesized to smooth the annual cycle. In winter, we can see positive geopotential forcing along 90° E, 120° W, and 0° E and the negative forcing along 120° E and 60° W in response to the topographic forcing as shown in Fig. 2. The barotropic forcing is weak in magnitude during summer. The anomaly of the forcing $f_i' = f_i - \tilde{f}_i$ is quite noisy as inferred from the example of Fig. 3. Approximately a half of the variance of f_i' is explained by the linear regression of $\mathbf{A}_{ij}w_j$ in (6). It is demonstrated (not shown) that the perfect-twin model experiments with the S-Model result in the same long predictability as in B-model.

Figure 16 illustrates an example of the actual forecasting for the Pacific blocking discussed in Fig. 1. Time integration is started from 1200Z, March 7, 1997. No initialization nor ensemble technique is applied for this forecasting experiment. A ridge developed over the east Pacific on March 11 as in observation, but the ridge is too weak to overturn the positive and negative vorticity field. The synoptic eddies are not excited much in the S-Model, and the mid-latitude jet tends to be broadened due to the lack of the momentum supply by baroclinic eddies.

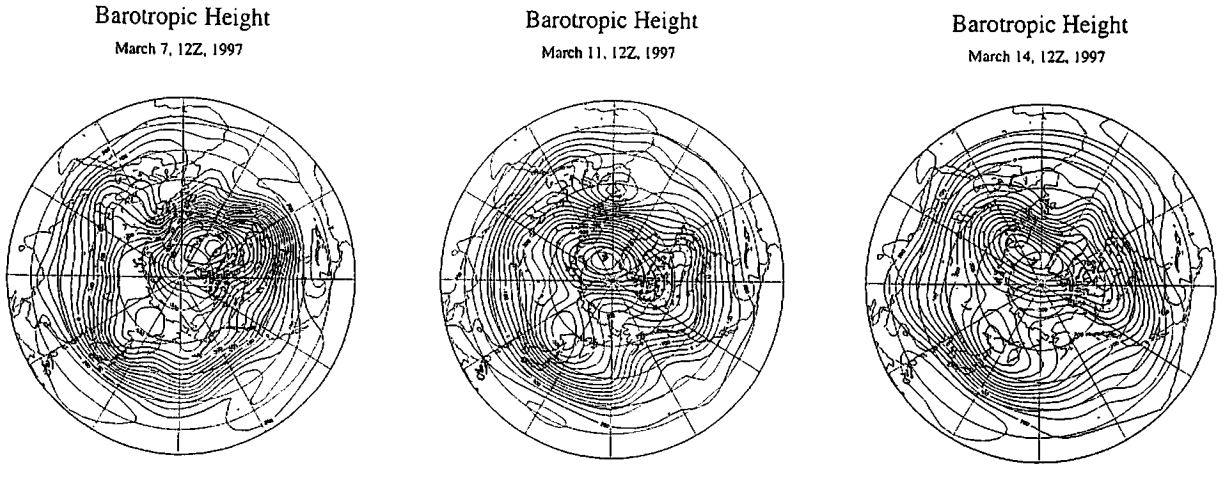

Fig. 16 A forecasting experiment of the real atmosphere as in Fig. 4. by the S-Model. The model equation with the external forcing of (6) is integrated from the initial condition of 1200Z on March 7. Distributions of the geopotential heights are plotted for 1200Z on (a) March 7, (b) March 11, and (c) March 14, 1997.

The failure of producing blocking on March 14 may be partly related to the weak synoptic eddies in the S-Model.

The forecasting experiment of the real atmosphere is repeated 23 times with the S-Model for the period from December 1996 to March 1997 using the GANAL/JMA data. The result of anomaly correlations for the forecasting experiments is plotted in Fig. 17. The thick line in the upper figure is the average of the 23 samples in the lower figure which are randomly chosen from the experiment period. The dotted line in the upper figure is for the persistence forecast. The mean anomaly correlation crosses the 0.6 line at about 3.0 day for the S-model. The result shows that the model has a predictability to some extent, but is not satisfactory compared with the present standard of operational forecasting models. The S-Model still has a considerable climate bias. The energy spectrum indicates weaker synoptic eddies. Yet, the major difficulty is contained in the complexity of the external forcing f_i. The accurate parameterization of the external forcing is the key problem to improve the S-Model for the successful forecasting.

According to the analysis of the forecasting error, it is found that the errorneous baroclinic instability parameterization and the low-frequency anomaly in the forcing are the main cause of the forecasting error. For this reason, and considering possible factores of error, we improve the S-Model by (a) adding a complex conjugate term as seen in (9), (b) evaluating matrices in (9) using only winter (DJF) data, and (c) adjusting the climate for the specific winter. Figure 18 illustrates the result of the anomaly correlation for prediction starting from 27 January 1989. The forecasting is repeated 20 times for different initial conditions for the 4 times daily data during 27 to 31 January. The result shows that the actual predictions have improved a lot, exceeding the mean predictability of about 8 days. Therefore, the S-Model may be useful as the extended range prediction model by a further improvement in the parameterization of the low-frequency variability such as SST forcing.

6. Concluding remarks

It has long been stated that the deterministic atmospheric predictability may be of the order of two weeks due to the chaotic nature of nonlinear fluid systems. Even if we can have a

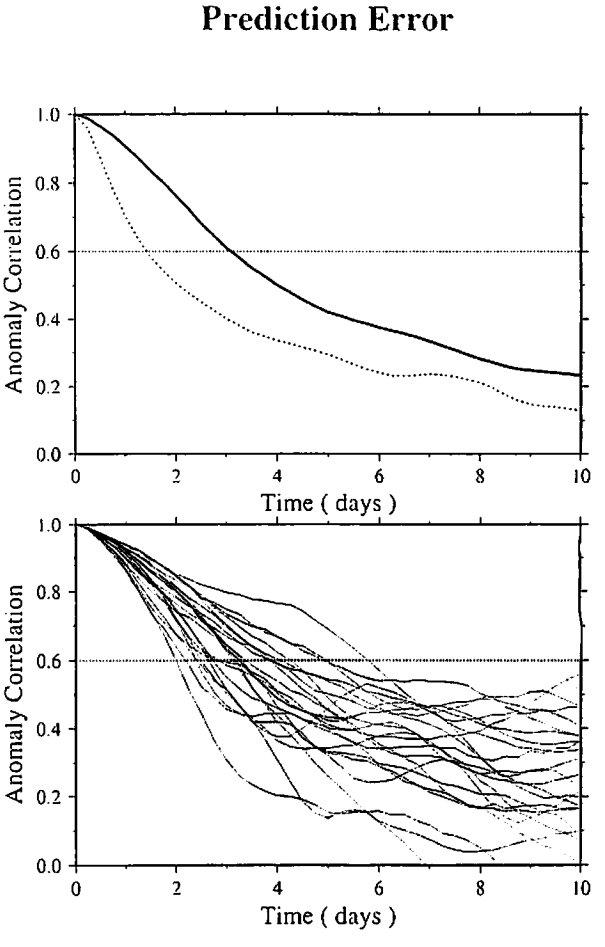

Fig. 17 (a): Mean anomaly correlation of geopotential heights for the 23 samples of the real forecasts by the S-Model (solid line) and corresponding persistence forecasting (dotted line). (b): The 23 individual samples of the anomaly correlation for the forecasting experiments with the S-Model. The experiments are carried out for the period from December 1996 to March 1997 using the GANAL/JMA data.

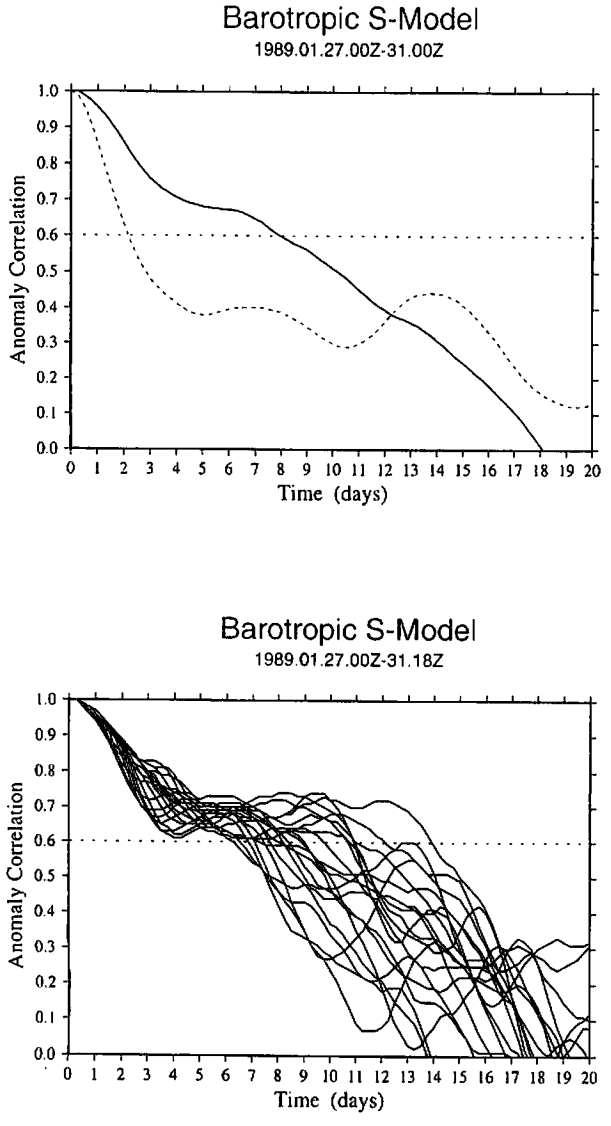

Fig. 18 Mean (a) and the 20 individual samples (b) of the anomaly correlation for the forecasting experiments with the improved S-Model with (9). The experiments are carried out for the period from 27 to 31 January 1989 using the NCEP-NCAR data.

perfect prediction model, a deterministic, medium-range weather forecast has been pessimistic beyond the chaotic barrier of two weeks (see Chen 1989). However, the possibility still remains to predict some averaged quantities. In this study, the predictability of the vertical mean state (barotropic component) of the atmosphere is examined by conducting perfect-twin model experiments.

In the first part of the paper, we evaluated the barotropic-baroclinic interactions from the observations during a pronounced blocking event in the north Pacific. Given the barotropic-baroclinic interactions as the external forcing, the barotropic model is integrated with respect to time. The model is referred to as a pseudo-perfect model (P-Model) since the perfect forcing is provided diagnostically from observations. It is demonstrated that the model accurately simulates the life-cycle of the blocking event in the real atmosphere. We found that the present model accurately follows the trajectory of the real atmosphere not just for a week, but for a hundred days after the initial date, as long as the correct external forcing is provided. The result may be non-trivial, since the model should contain a certain amount of noise during the computation which is bigger than the butterfly effect discussed by Lorenz.

Based on the result of the P-Model, the pseudo-perfect-twin model experiments are then conducted to examine how the initial error grows. The result shows that the predictability increases 10 days when the initial error energy is reduced by 1/10. Predictability limit is inversely proportional to the logarithm of the error energy level. This implies that the predictability increases as long as the initial error decreases as noted by Lorenz (1969) for 2-D turbulent flows. This property of the barotropic model can be useful for the actual medium-range forecasting. Since the model predicts the vertical mean quantities, the local observational error may be reduced in proportion to the square root of the total number of the data samples. Hence, the result suggests that the vertical mean state may be predictable beyond two weeks "if" we can have a perfect model and sufficient number of observations in the vertical. However, it must be a big "if" as a working hypothesis.

In the second part of the paper, we integrated

the B-Model which computes the forcing internally within the model. The parameterization of baroclinic instability is introduced as an important factor to excite synoptic eddies, which is essential in the model atmosphere to simulate the realistic blocking by means of the inverse energy cascade. A perfect-twin model experiment is then conducted with the B-Model for the life-cycle of a blocking appeared in the model atmosphere. Namely, we superimposed a small error on the solution trajectory two weeks before the blocking formation in the model. We demonstrated that the robust blocking life-cycle in the model atmosphere is reproduced using the initial data two weeks in advance despite the abundant initial noise. It is concluded that predicting the vertical mean of the atmosphere is less sensitive to the initial noise. A nonlinear fluid system is chaotic only when the nonlinear system has strong dynamical instability which grows the initial error. The result implies that the nonlinearity is not the essential factor of chaos, but the dynamical instability contained in the system is essential for it. For this reason, the vertical mean of the atmosphere is much predictable than we thought even though it is a highly nonlinear system. The result of present study suggests that predicting the vertical mean of the atmosphere can be one of the viable approaches to the medium-range weather prediction, provided that the barotropic-baroclinic interactions are accurately parameterized.

Using a quasi-geostrophic barotropic model, similar long predictability is discussed by previous studies by Leith (1971), Leith and Kraichnan (1972), Basdevant et al. (1981), Holloway (1983), and Vallis (1983). Among those, Vallis (1983) shows the longest predictability of 25 days. It is shown, however, that the predictability of the present barotropic model is much longer than those by the quasi-geostrophic barotropic model. The parameterized baroclinic instaibity in this study, even though it is linear and simple, causes the error to grow fast with the e-folding time of 2 to 3 days. Yet, the error growth is much slower than that. It is the nonlinearity in the 2-D flow that reduces the error growth. The inverse energy cascades seem to be important to understand the phenomenon. Holloway (1983) demonstrated that initial error in small scales also cascades up to planetary waves similar to the energy itself in the 2-D turbulence. The planetary waves are strongly forced by topography maintaining stationary Rossby waves. It seems that error energy cascading up to planetary waves collapses by the balance of the topographic forcing and Ekman damping. Further study is necessary to support this speculation.

In the last part of the paper, we demonstrated an example of actual forecasting for the Pacific blocking using the S-Model, in which a best linear fit of the external forcing is obtained from 17 years of the NCEP-NCAR reanalysis. The mean anomaly correlation for the S-Model indicates that the meaningful predictability is about 3 day. However, the S-Model can be improved by introducing the complex conjugate term of the state variable w_i. As a result, we found that the predictability extends up to 8 days for the improved S-Model.

Comparing the fact of the less chaotic features discussed above, the result of the short predictability for the real atmosphere implies that all difficulty associated with the chaos in the operational forecasting is now contained in the complexity of the external forcing f_i. Hence, the question is to obtain the suitable functional form for the non-autonomous system of $f_i(w_i, \tau)$. A large fraction of f_i seems to vary independently of the state variables w_i, at least, in the linear framework. Since we can assess both of f_i and w_i diagnostically from observations, one direction to improve the model is to formulate the higher order nonlinear terms in the Taylor series approximation of f_i. Another direction is to include external

parameters such as sea surface temperature (SST), soil moisture, and so on by means of the multiple regression technique. It is demonstrated that the diurnal cycle and a higher-frequency random noise in the forcing is less sensitive to the forecasting. They may be treated as random noise. Hence, the problem is to formulate the slowly varying part of the forcing in terms of the internal and external parameters. It is importnat to note that the difficulty in the S-Model is now regarded as a model error rather than chaos.

Acknowledgments

This research was supported by the Grant-in-Aid for Scientific Research, Japanese Minstry of Education, Science, Sport and Culture, No. 09640518. Partial support came from the Environmental Reseach Fund from Asahi Beer, Japan. The author appreciates Ms. K. Honda for her technical assistance.

REFERENCES

Baer, F., 1972: An alternate scale representation of atmospheric energy spectra. *J. Atmos. Sci.*, **29**, 649-664.

Basdevant, C., B. Legras, and R. Sadourny, 1981: A study of barotropic model flows: Intermittency, waves and predictability. *J. Atmos. Sci.*, **38**, 2305-2326.

Bengtsson, L., 1985: Medium-range forecasting at the ECMWF. Issues in Atmospheric and Oceanic Modeling. *Advances in Geophysics*, **28** (eds. S. Manabe) Academic Press, 3-54.

Chen, W. Y., 1989: Estimate of dynamical predictability from NMC DERF experiments. *Mon. Wea. Rev.*, **117**, 1227-1236.

Dalcher, A. and E. Kalnay, 1987: Error growth and predictability in operational ECMWF forecasts. *Tellus*, **39A**, 474-491.

Edmon, H. J., B. J. Hoskins and M. E. McIntyre, 1980: Eliassen-Palm cross section for the troposphere. *J. Atmos. Sci.*, **37**, 2600-2616.

Holloway, G., 1983: Effects of planetary wave propagation and finite depth on the predictability of atmosphere. *J. Atmos. Sci.*, **40**, 314-327.

Hoyer, J.-M., and R. Sadourny, 1982: Closure modeling of fully developed baroclinic instability. *J. Atmos. Sci.*, **39**, 707-721.

Kalnay, E., M. Kanamitsu, and W.E. Baker, 1990: Global numerical weather prediction at the National Meteorological Center. *Bull. Amer. Meteor. Soc.*, **71**, 1410-1428.

——, S.J.Lord, and R.D. McPherson, 1998: Maturity of operational numerical weather prediction: Medium range. *Bull. Amer. Meteor. Soc.*, **79**, 2753-2769.

Kasahara, A., 1977: Numerical integration of the global barotropic primitive equations with Hough harmonic expansions. *J. Atmos. Sci.*, **34**, 687-701.

Leith, C. E., 1971: Atmospheric Predictability and two-dimensional turbulence. *J. Atmos. Sci.*, **28**, 145-161.

——, and R. H. Kraichnan, 1972: Predictability of turbulent flows. *J. Atmos. Sci.*, **29**, 1041-1058.

Lorenz, E. N., 1963: Deterministic nonperiodic flow. *J. Atmos. Sci.*, **20**, 130-141.

——, 1969: The predictability of a flow which possesses many scales of motion. *Tellus*, **21**, 289-307.

——, 1985: The growth of errors in prediction. *Turbulence and Predictability in Geophysical Fluid Dynamics and Climate Dynamics*, North-Holland, 243-265.

Miyakoda, K., J. Sirutis and J. Ploshay, 1986: One-month forecast experiments-without anomaly boundary forcings. *Mon. Wea. Rev.*, **114**, 2363-2401.

Molteni, F., R. Buizza, T.N. Palmer, and T. Petroliagis, 1996: The ECMWF ensemble prediction system: Method and validation. *Quart. J. Roy. Meteor. Soc.*, **122**, 73-119.

Rhines, P.B., 1975: Waves and turbulence on a beta-plane. *J. Fluid Mech.*, **69**, 417-443.

Ringler, T.D. and K. H. Cook, 1999: Understanding the seasonality of orographically forced stationary waves: Interaction between mechanical and thermal forcing. *J. Atmos. Sci.*,

56, 1154-1174.

Salmon, R., 1980: Baroclinic instability and geostrophic turbulence. *Geophys. Astrophys. Fluid Dyn.* **15**, 167-212.

Satoh, M., 1994: Hadley circulations in radiative-convective equilibrium in an axially symmetric atmosphere. *J. Atmos. Sci.*, **51**, 1947-1968.

Shukla, J., 1985: Predictability. Issues in Atmospheric and Oceanic Modeling. *Advances in Geophysics,* **28** (eds. S. Manabe) Academic Press, 87-122.

Shutts, G. J., 1986: A case study of eddy forcing during an Atlantic blocking episode. *Adv. in Geophys.* **29**, 135-162.

Stone, P. H., 1978: Baroclinic adjustment. *J. Atmos. Sci.*, **35**, 561-571.

Tanaka, H. L., 1991: A numerical simulation of amplification of low-frequency planetary waves and blocking formations by the upscale energy cascade. *Mon. Wea. Rev.*, **119**, 2919-2935.

——, 1995: A life-cycle of nonlinear baroclinic waves represented by 3-D spectral model. *Tellus*, **47A**, 697-704.

——, 1998: Numerical simulation of a life-cycle of atmospheric blocking and the analysis of potential vorticity using a simple barotropic model. *J. Meteor. Soc. Japan,* **76**, 983-1008.

——, and E.C. Kung, 1988; Normal mode energetics of the general circulation during the FGGE year. *J. Atmos. Sci.*, **45**, 3723-3736.

——, and K. Kimura, 1996: Normal model energetics analysis and the intercomparison for the recent ECMWF, NMC, and JMA global analyses. *J. Meteor. Soc. Japan,* **74**, 525-538.

Thompson, D. W. J. and J. M. Wallace, 1998: The Arctic oscillation signature in the wintertime geopotential height and temperature field. *Geophys. Res. Lett.*, **25**, 1297-1300.

Toth, Z. and E. Kalnay, 1997: Ensemble forecasting at NCEP and the breeding method. *Mon. Wea. Rev.*, **125**, 3297-3319.

Vallis, G. K., 1983: On the predictability of quasi-geostrophic flow: The effect of beta and baroclinicity. *J. Atmos. Sci.*, **40**, 10-27.